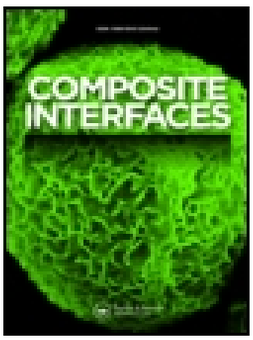

Composite Interfaces

ISSN: (Print) (Online) Journal homepage: https://www.tandfonline.com/loi/tcoi20

Improved mechanical and high-temperature electromagnetic wave absorption properties of $SiC_f/BN/AlPO_4$ composites with absorber multiwalled carbon nanotubes

Feng Wan , Jianhui Yan & Hongmei Xu

To cite this article: Feng Wan , Jianhui Yan & Hongmei Xu (2020): Improved mechanical and high-temperature electromagnetic wave absorption properties of $SiC_f/BN/AlPO_4$ composites with absorber multiwalled carbon nanotubes, Composite Interfaces, DOI: 10.1080/09276440.2020.1812336

To link to this article: https://doi.org/10.1080/09276440.2020.1812336

COMPOSITE INTERFACES
https://doi.org/10.1080/09276440.2020.1812336

Taylor & Francis
Taylor & Francis Group

Improved mechanical and high-temperature electromagnetic wave absorption properties of $SiC_f/BN/AlPO_4$ composites with absorber multiwalled carbon nanotubes

Feng Wan [a,b], Jianhui Yan[a,b] and Hongmei Xu[a,b]

[a]School of Materials Science and Engineering, Hunan University of Science and Technology, Xiangtan, Hunan, China; [b]Hunan Provincial Key Laboratory of Advanced Materials for New Energy Storage and Conversion, Hunan University of Science and Technology, Xiangtan, Hunan, China

ABSTRACT

An electromagnetic wave absorbing material acting from 8.2 to 12.4 GHz (X-band) is fabricated by mixing BN-coated SiC fiber with $AlPO_4$ matrix, and using multiwalled carbon nanotubes (MWNCTs) as the absorber. The effect of temperature on the microstructure of BN interface is disclosed by XRD and FT-IR characterizations. The crystallinity of BN increased with elevated temperature. The fracture strength of $SiC_f/BN/AlPO_4$ composites rise from 175 to 350 MPa and the fracture displacement was elevated from 0.25 to 0.7 mm. The increasing complex permittivity of $SiC_f/BN/AlPO_4$/MWCNTs composites in the temperature range of 25–600 °C is ascribed to the shortened electron polarization-relaxation time and improved electrical conductivity. Attenuation constant and input impedance are chosen to discuss the reflection loss of the composites. Finally, a 4.2 GHz absorbing bandwidth below −8 dB is achieved with 3.1 mm thickness in the range of 25–600 °C.

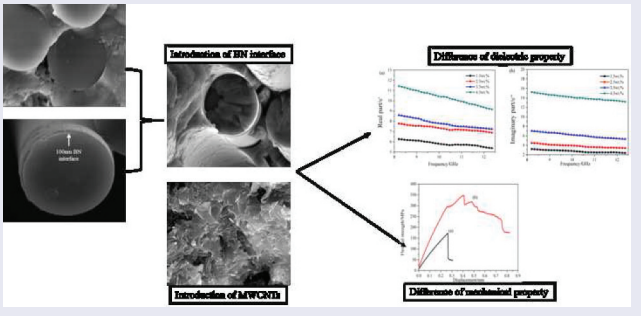

ARTICLE HISTORY
Received 1 April 2020
Accepted 17 August 2020

KEYWORDS
SiC fiber; $ALPO_4$ matrix; BN interface; microwave absorber

1. Introduction

Electromagnetic wave absorbing materials are designed to decrease the reflected electromagnetic wave by absorbing electromagnetic wave and transforming it into other energy, which have achieved extensive focus in aerospace and military fields [1–7]. Currently,

CONTACT Feng Wan wanfenghkd@163.com School of Materials Science and Engineering, Hunan University of Science and Technology, Xiangtan, Hunan 411201, China

good application in high-temperature environments is a main topic of the research for electromagnetic wave absorbing properties.

Ceramic matrix composites (CMCs) are designed to act as structural materials by overcoming the brittleness of pure ceramics, show casing advantageous high temperature stability and stiffness. Currently, CMCs receive increasing interest and are developed as high temperature wave absorbing materials [8–13]. Researchers have especially paid much attention to construct SiC fiber reinforced CMCs due to their high toughness, such as SiC_f/SiC composites [14–17], SiC_f/lithium–aluminum–silicate (LAS) composites [18], and SiC_f/aluminum phosphate ($AlPO_4$) composites [19–21].

CVI (Chemical vapor infiltration) or PIP (Precursor infiltration and pyrolysis) methods are usually employed to prepare SiC_f/SiC composites. Although SiC_f/SiC composites have good mechanical properties, the SiC matrix from PIP or CVI process is rich in carbon content, leading to a high conductivity and a strong electromagnetic wave reflection for SiC_f/SiC composites [22–24]. Compared with SiC_f/SiC composites, the SiC fiber reinforced insulated oxide matrix (SiO_2, Mullite, LAS) composites have a low dielectric constant and weak electromagnetic wave reflection, but the high temperature sintering process damages the SiC fiber structure and leads to poor mechanical properties. SiC_f/$AlPO_4$ composites not only show excellent mechanical properties, but also a low dielectric constant, allowing adjustments of the wave absorbing property. Moreover, SiC_f/$AlPO_4$ composites are fabricated by a low-temperature curing process, which is more economical and environmentally friendly.

In this paper, SiC_f/BN/$AlPO_4$/MWCNTs composites are prepared by lamination with MWCNTs for fine tuning dielectric property and with BN interface for improving the mechanical property. The complex permittivity is investigated from 25 to 600°C and in X-band. The reflection loss of SiC_f/BN/$AlPO_4$/MWCNTs composites in the X-band is simulated.

2. Experiment

2.1. Experimental materials

SiC fibers were provided by National University of Defense Technology (China), The properties of SiC fibers are shown in Table 1. MWCNTs with diameter of 30–90 nm, length of 5–10 μm, and purity greater than 96% were chosen.

2.2. Preparation of BN interface

The solvent was prepared by mixing 100 mL deionized water with 200 mL methanol. About 3 g of boric acid (H_3BO_3) and 27 g of urea ($CO(NH_2)_2$) were mixed into the solvent, which was ultrasonically treated for 20 min to obtain the precursor fluid of BN.

Table 1. Properties of KD-1 fibers.

Fiber type	Diameter (μm)	Density (g/cm^3)	Tensile strength (MPa)	Electric conductivity (S/cm)	C/Si ratio
KD-1	14–16	2.54	1800–2200	2–3	1.25

After 20 min ultrasonically clean in alcohol solution, SiC cloths were put in the precursor fluid of BN. Then these cloths were drawn out from the solution with a roller constantly running at 60 rpm. Finally, under a nitrogen atmosphere, these cloths were placed in a vacuum furnace and pyrolyzed with heating rate 8°C/min up to 800°C, 900°C, 1000°C, and 1100°C, respectively.

2.3. Preparation of SiC_f/BN/$AlPO_4$/MWCNTs composites

The preparation process of $Al(H_2PO_4)_3$ solution, which was used to form $AlPO_4$ matrix, can be found in Ref [21]. Four different amounts of MWCNTs (1.5, 2.5, 3.5, and 4.5 wt.%) were add into the $Al(H_2PO_4)_3$ solution. A uniform slurry is obtained after 3 h ball milling. Next, some sheets of BN-coated SiC cloths were dipped in the slurry and were then hot pressed to obtain SiC_f/BN/$AlPO_4$/MWCNTs composites, as depicted in Figure 1. The final dimension of the prepared composites was approximately 50 mm^l × 50 mm^w × 3 mm^t.

2.4. Characterization

The BN structure was investigated by Fourier transform infrared spectrum (Nicolet Nexus 670 with the resolution of 4 cm^{-1} and the wavelength of 400–4000 cm^{-1}, the KBr pellet method is used to prepare the sample) and X-ray diffraction (X' Pert Pro, Philips, Netherlands), using Cu Kα (λ = 0.154 nm) radiation and scanning from 15° to

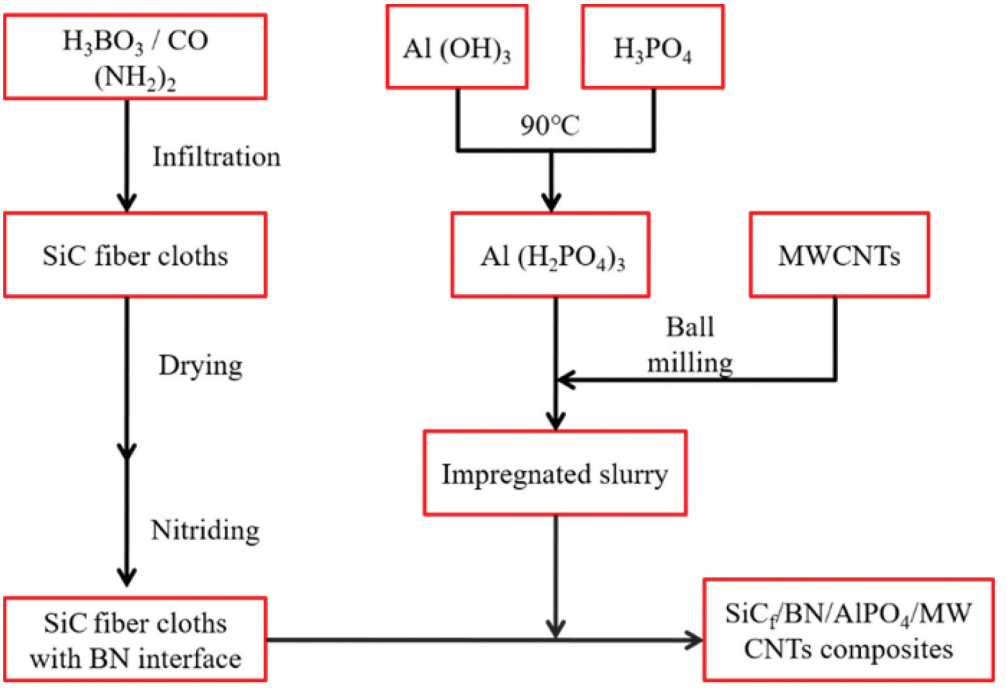

Figure 1. Preparation route of SiC_f/BN/$AlPO_4$/MWCNTs composites.

90°. The morphologies of BN interface and $SiC_f/AlPO_4$ composites were characterized by SEM (ZEISS Supra55).

The flexural strength (σ) of $SiC_f/BN/AlPO_4$ composites was determined by three-point bending test and was calculated based on Equation (1):

$$\sigma = \frac{3PL}{2wt^2} \tag{1}$$

where L is the length of support span, t is specimen thickness, w is specimen width, and P is load at a point of deflection of a load-displacement curve in test. The composites sample was cut and polished to 40 $mm^l \times 4\ mm^w \times 3mm^t$.

The dielectric property of the $SiC_f/BN/AlPO_4$/MWCNTs composites was measured using a vector network analyzer (E8362B) based on the waveguide method in X-band, shown in Ref [25].

The DC (direct current) conductivity (σ_{dc}) of $SiC_f/BN/AlPO_4$/MWCNTs composites was measured using a simple method. Some samples (22.86 $mm^l \times 10.16\ mm^w \times 3\ mm^t$) were covered with a conductive Ag paint on two parallel surfaces. Then, σ_{dc} of the samples in the thickness direction was calculated according to Equation (2) [26]:

$$\sigma_{dc} = L/R_eS \tag{2}$$

where R_e is the electric resistance, L is the 3 mm thickness, and S is the surface area (22.86 mm × 10.16 mm).

3. Results and discussion

3.1. Effect of temperature on the microstructure of BN interface

Figure 2 shows the XRD patterns of BN products prepared at four temperatures of 800°C, 900°C, 1000°C, and 1100°C. The intensity of diffraction peak at 26.5° (2θ) corresponding to turbostratic BN (t-BN) [27] increases gradually when the temperature rises from 800°C to 1100°C. With increasing temperature, the diffraction peak at 26.5° (2θ) becomes narrower and sharper, proving that the crystalline degree of t-BN is improved. At 800°C, the formation of t-BN is not obvious. At 900°C, there is the existence of H_3BO_3, proving that the formation of t-BN is incomplete. At high temperature, the decomposition of H_3BO_3 brings holes to the BN interface and decreases the antioxidization effect of BN interface. So, it is not suitable to prepare BN interface at 800°C and 900°C.

Figure 3 shows the Fourier transform infrared spectrum of reaction products at 1000°C and 1100 °C. A sharp and broad absorption peak is seen to occur at 800 cm^{-1} and 1400 cm^{-1} under both temperatures. The peak near 1400 cm^{-1} and 800 cm^{-1} should be ascribed to the in-plane B-N TO models of the sp^2-bonded BN and the B-N-B bonding vibration out of the plane, respectively [28]. These results from Figures 1 and 2 prove that pure t-BN was formed above 1000°C. In order to decrease the damage to the SiC fiber during the preparation of BN interface, the temperature is chosen to be 1000°C [29].

The surface morphologies of original and coated SiC fibers at 1000°C are investigated by SEM, shown in Figure 4. As seen from Figure 4(a), the surface of original SiC fibers is smooth and shows few defects. It is revealed in Figure 4(b–c) that the surfaces of SiC

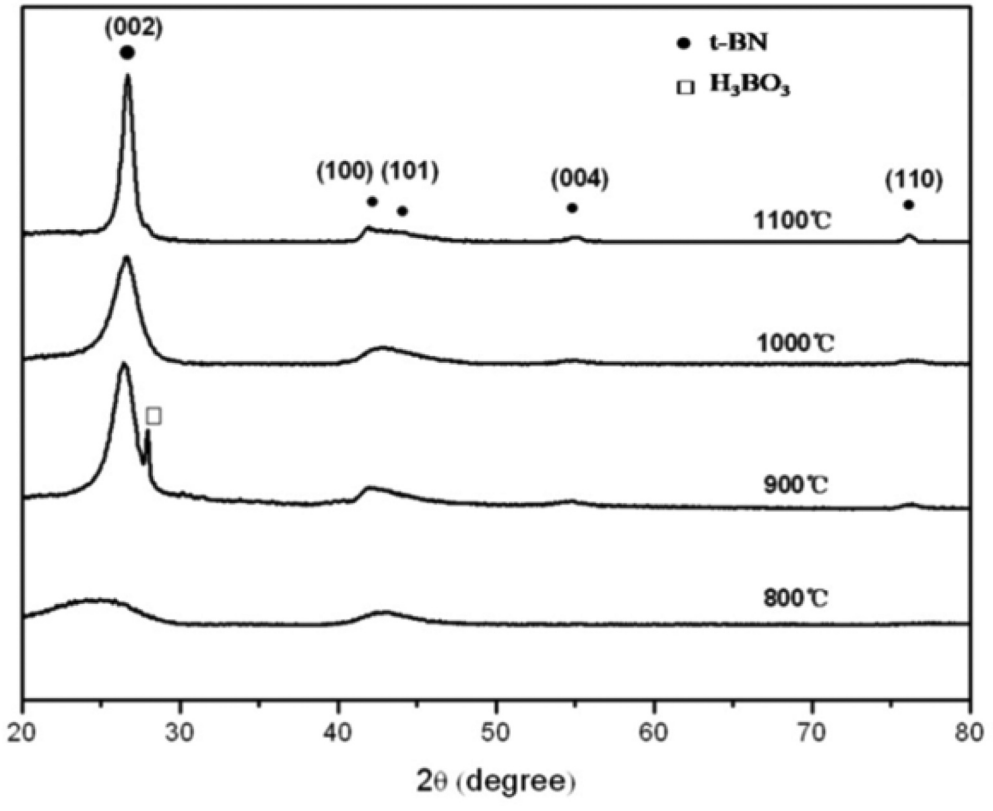

Figure 2. The XRD patterns of BN interface prepared at different temperatures.

fibers with interfaces are relatively smooth and uniform, and no bridging is detected, representatively. Bridging between fibers can affect deposition of matrix and lead to nonoptimal mechanical properties in consequence of stress concentration on the defects. To minimize stress concentration and have the correct crack deflection behavior, a proper surface morphology (Interfacial roughness) of interphase for composites is necessary. The smooth and uniform BN interfaces prepared at 1000°C decrease the stress concentration and offer the interfacial friction force in $SiC_f/BN/AlPO_4$ composites, which are suitable to be applied as interfaces.

3.2. Effect of BN interface an MWCNTs on the mechanical property of SiC_f /BN/$AlPO_4$ composites

$SiC_f/AlPO_4$ composites (50 mml × 50 mmw × 3 mmt) with and without BN interface are cut into six samples (40 mml × 4 mmw× 3mmt) to test the flexural strength. The final flexural results are supported by the minimum value in six samples. The flexural strength-fracture displacement curves of BN-coated and BN-uncoated $SiC_f/AlPO_4$ composites are reflected in Figure 5. A low 170 MPa in flexural strength is achieved for SiC_f /$AlPO_4$ composites without BN interface in curve a, showing a short fracture displacement of 0.25 mm. The fracture displacement is determined from 0 in X axis to the value

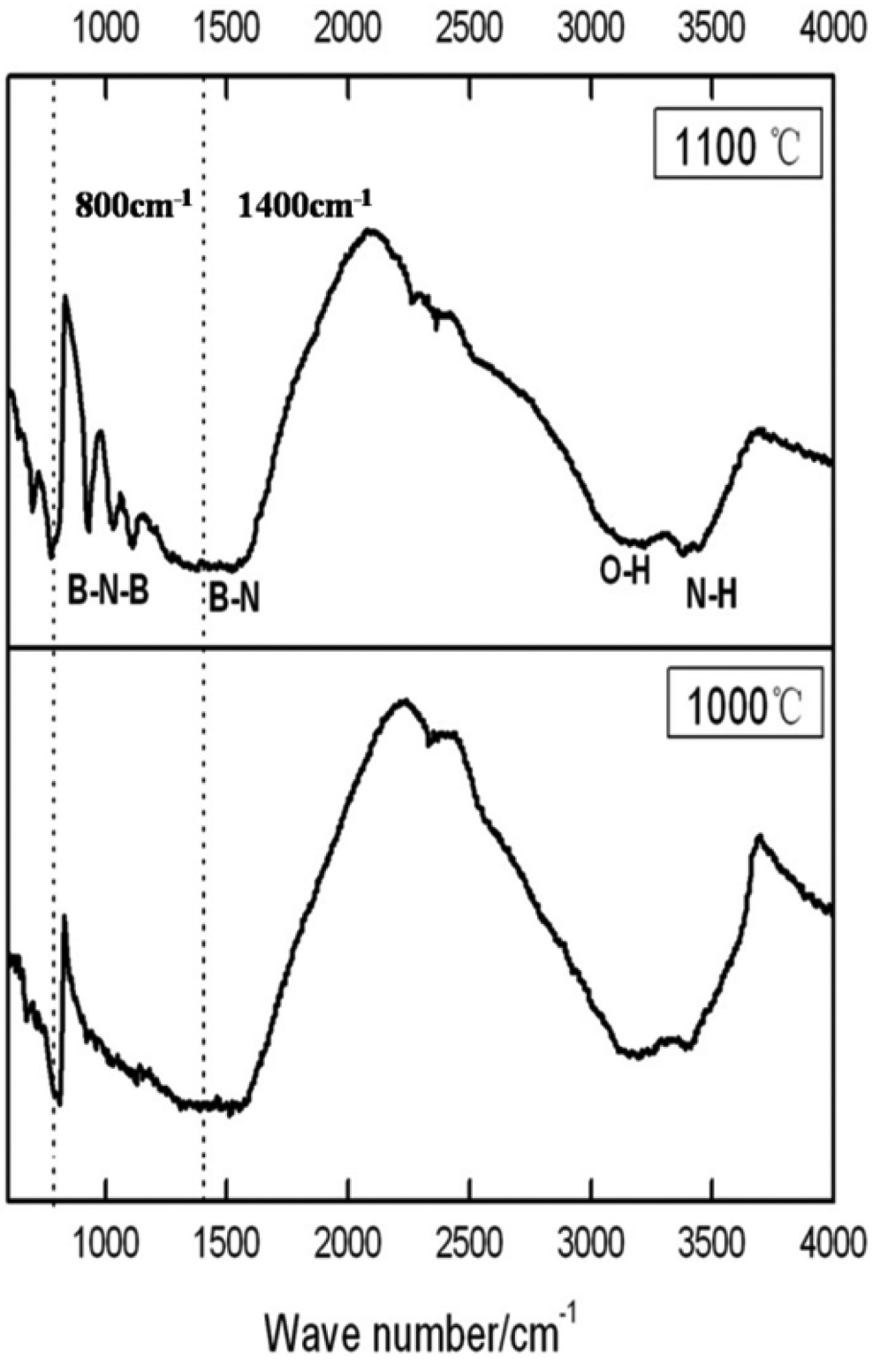

Figure 3. FT-IR spectra of products from urea and boric acid at 1000°C and 1100°C.

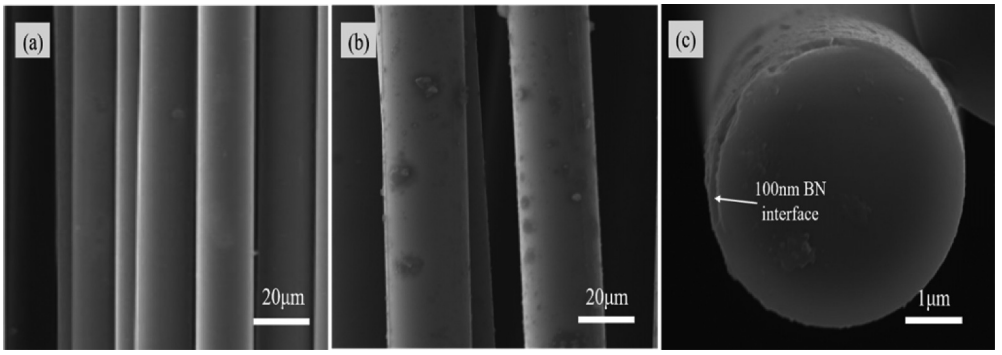

Figure 4. SEM images of pristine SiC fiber (a) and SiC fiber coated with BN at 1000°C (b, c).

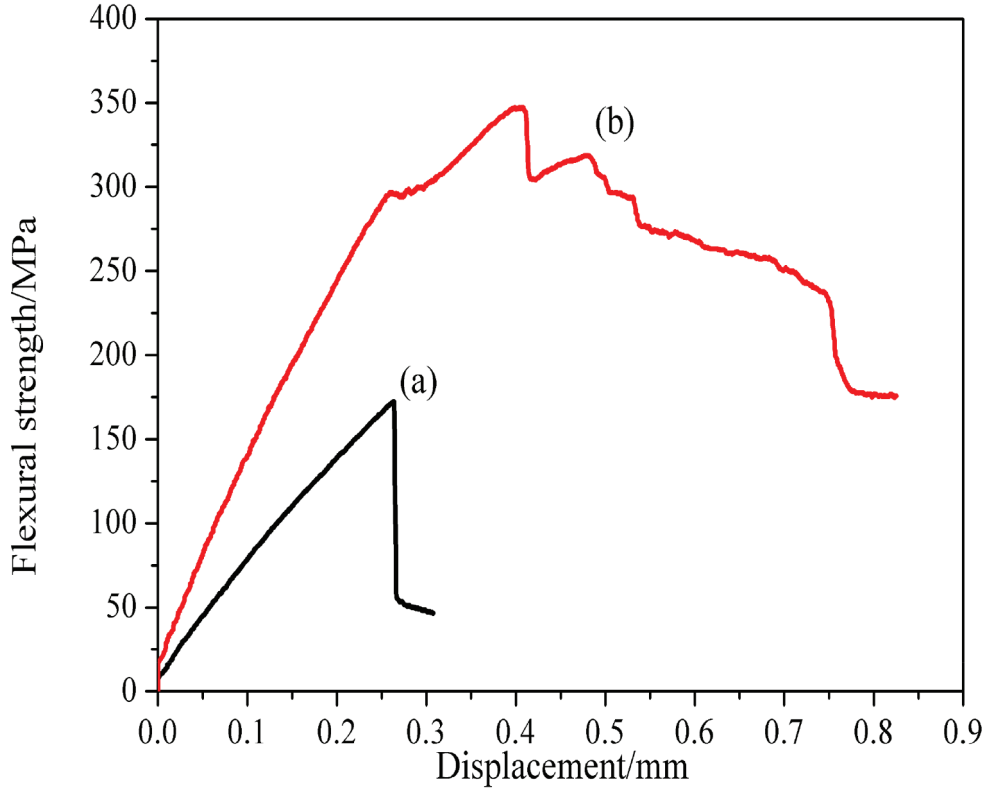

Figure 5. Stress-displacement curves of $SiC_f/AlPO_4$ composites: (a) without BN interface and (b) with BN interface.

corresponding to the maximal flexural strength. The sample cracks in a catastrophic and brittle manner due to the strong bonding strength between $AlPO_4$ matrix and SiC fiber. After the introduction of BN interface at 1000°C, the $SiC_f/BN/AlPO_4$ composites display an obviously toughened fracture behavior, shown in curve b. A high 350 MPa in flexural

strength and a long fracture displacement of 0.4 mm are obtained, which proves that much more energy during fracture process is consumed. Multiple fiber reinforcing mechanisms, including fiber debonding, crack deflection and fiber pullout may contribute to the enhanced mechanical strength, as supported by SEM results in Figure 6.

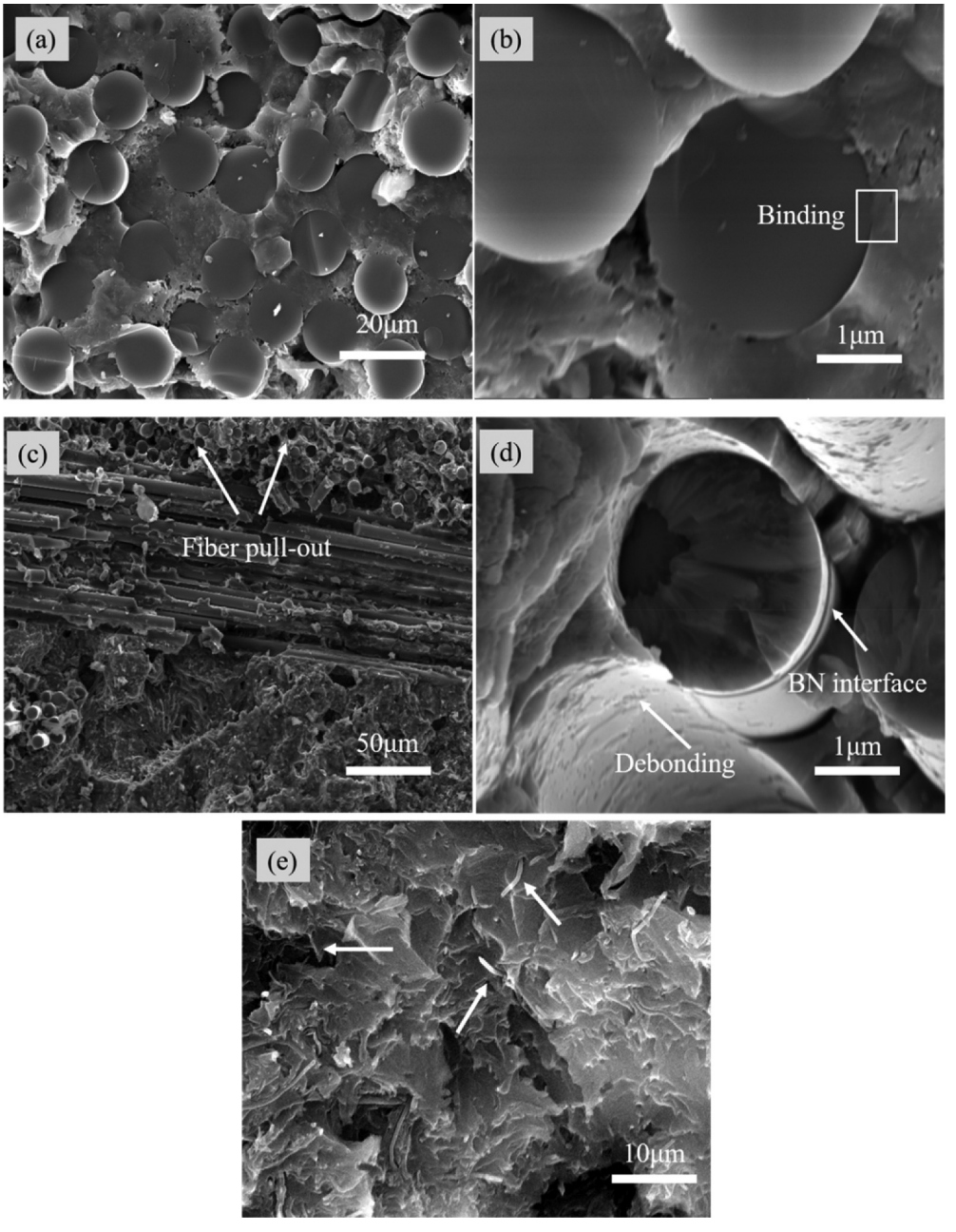

Figure 6. The surface morphologies of $SiC_f/AlPO_4$ composites: (a) and (b) without BN interface, (c) – (e) with BN interface at 1000°C.

Figure 6 shows the fracture surface morphologies of BN-coated and BN-uncoated SiC_f /$AlPO_4$ composites. The fracture surface of BN-uncoated SiC_f/$AlPO_4$ composites is relatively even and displays little fiber debonding and fiber pullout due to the strong SiC fiber binding. After SiC fiber surface modification with BN at 1000°C, SEM of fracture surfaces show considerable amounts of voids, fiber debonding, and topographical uneven surface in Figure 6(c, d).

Fiber strength and interfacial binding strength determined the mechanical properties of SiC_f/$AlPO_4$ composites. Without BN interface, the strong interfacial binding strength makes the fiber reinforced mechanisms fail, energy cannot be deflected and caused the brittle fractures. The introduction of BN interface not only protects SiC fiber from being damaged, but also decreases the interfacial binding strength and enhances the compatibility between fiber and matrix. By toughening mechanisms like fiber debonding, cracks deflection and fiber pullout, the energy of cracks propagation in the matrix is consumed gradually.

Not only BN interface makes much contribution, but also the introduction of MWCNTs plays a role in improving the flexural strength. It is found in Figure 6(e) that many MWCNTs are pullout from matrix and bridged between matrix. During pullout and bridging, much energy of cracks propagation is consumed.

As a result, the SiC_f/BN/$AlPO_4$ composites exhibit a high flexural strength, a long fracture displacement and high fracture energy due to the introduction of BN interface and MWCNTs, reflected in Figure 5(b).

3.3. Effect of MWCNTs content on the dielectric property of SiC_f/BN/$AlPO_4$ composites

Figure 7 shows the values of complex permittivity for SiC_f/$AlPO_4$ composites with and without BN interface. Real part is ε' and imaginary part is ε″. It can be found that ε' has a slight increase while ε″ shows little change after coating BN layer.

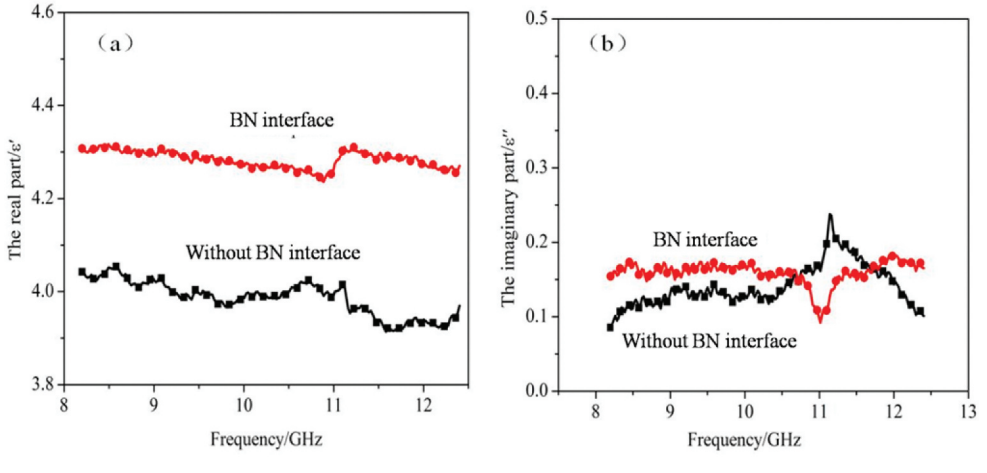

Figure 7. The (a) real part/ε' and (b) imaginary part/ε″ of SiC_f/$AlPO_4$ composites with and without BN interface.

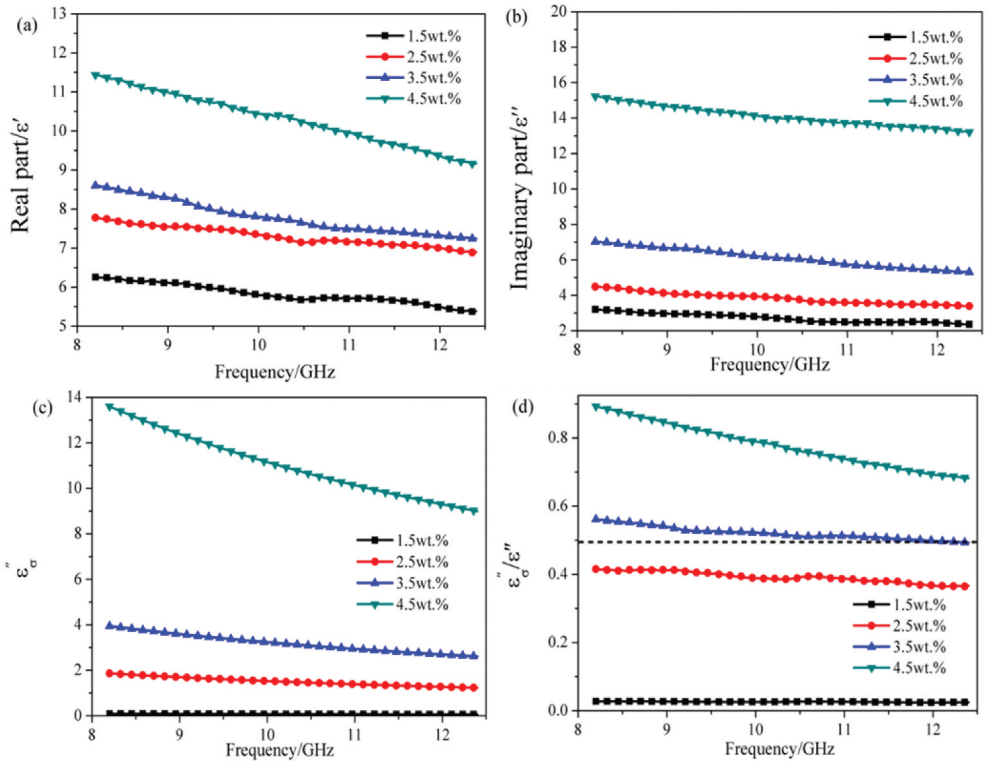

Figure 8. (a) real part/ε′, (b) imaginary part/ε″, (c) ε_σ'' and (d) $\varepsilon_\sigma''/\varepsilon''$ for $SiC_f/BN/AlPO_4$/MWCNTs composites with different amounts of MWCNTs.

The ε' and ε″ values for $SiC_f/BN/AlPO_4$/MWCNTs composites with different amounts of MWCNTs (1.5, 2.5, 3.5, and 4.5 wt. %) are reflected in Figure 8. Both the values of complex permittivity increase in the X-band with MWCNTs content changing from 0 to 4.5 wt. %, ε' value increasing from 3.9 ~ 4.0 to 9 ~ 11.5 and ε″ value increasing from 0.1 ~ 0.2 to 13.1 ~ 15.2.

ε' and ε″ can be calculated according to the Debye equation [30]:

$$\varepsilon' = \varepsilon_\infty + \frac{\varepsilon_s - \varepsilon_\infty}{1 + \omega^2\tau(T)^2} \tag{3}$$

$$\varepsilon'' = \varepsilon_\tau'' + \varepsilon_\sigma'' \tag{4}$$

$$\varepsilon_\tau'' = \frac{(\varepsilon_s - \varepsilon_\infty)\omega\tau(T)}{1 + \omega^2\tau(T)^2} \tag{5}$$

$$\varepsilon_\sigma'' = \frac{\sigma(T)}{\omega\varepsilon_0} \tag{6}$$

where ε_∞ is the permittivity at the high-frequency limit, ε_s is the static permittivity, ω is the angular frequency of $2\pi f$, ε_0 is the permittivity in the vacuum, $\tau(T)$ is the relaxation time of 8.85×10^{-12} F/m.

ε' is controlled by the polarization relaxation time, depicted in Equation (3). There are various electric polarizations such as space charge polarization, molecular or dipolar polarization, ionic polarization, atomic polarization, and electronic polarization. Electronic and atomic polarization is sure to take place in the microwave range. The space charge polarization in the GHz range is often ignored considering a long time to establish. So, the electronic polarization relaxation mainly leads to the increase of ε'. Highly conductive MWCNTs can serve as an electron transfer medium inside the SiC fiber reinforced $AlPO_4$ matrix. More electrons migrate and accumulate at the interfaces but some of these electrons cannot catch up with the alternating EM field, and thus the polarization relaxation occurs.

As described in Equation (4)-(6), both the relaxation time and electric conductivity play key roles in ε″. Table 2 shows that the electric conductivity of $SiC_f/BN/AlPO_4$ MWCNTs composites increases with increasing MWCNTs. The values of ε_σ'' and $\varepsilon_\sigma''/\varepsilon''$ can be calculated, depicted in Figure 8(c) and Figure 8(d), respectively. With 1.5 wt.% MWCNTs addition, the ε_σ'' value is small and $\varepsilon_\sigma''/\varepsilon''$ value is below 0.5, proving that the polarization mechanism controls the ε″. The increasing MWCNTs content makes the ε_σ'' and $\varepsilon_\sigma''/\varepsilon''$ values show an increasing tendency, which proves that the effect of electric conductance loss on the ε″ becomes more and more important. Especially, the values of $\varepsilon_\sigma''/\varepsilon''$ exceed 0.5 when MWCNTs content exceeds 3.5 wt. %.

When the MWCNTs are in contact with each other, proved by Figure 6(e), the free electrons transfer between nanotubes and direct current is formed, leading to electrical conductivity loss. More MWCNTs contact with each other or have closer distance, more continuous conduction paths are form or more hopping electrons are obtained, if the MWCNTs content is raised [31,32]. So, much more direct current is obtained, resulting in more electric conductivity loss [33]. These results are proved by Figure 8(c,d).

3.4. Effect of temperature on the microwave absorbing property of $SiC_f/BN/AlPO_4$/MWCNTs composites

At temperature between 25 and 600°C in X-band, the values of complex permittivity for $SiC_f/BN/AlPO_4$/MWCNTs composites with 1.5 wt. % MWCNTs are reflected in Figure 9. As depicted in Figure 9(a), ε' value changes from 6.5 to 5.4 at 25°C and 8 to 6.9 at 600°C in the X-band range. As is exhibited in Figure 9(b), the value of ε″ changes from 3.1 to 2.3 at 25°C and 4.6 to 3.2 at 600°C in the X-band range.

Figure 10 shows the calculated reflection loss of $SiC_f/BN/AlPO_4$/MWCNTs composites containing 1.5 wt.% MWCNTs in the range of 25–600°C. There are six different calculated thicknesses at each temperature: 2.6 mm, 2.8 mm, 3.0 mm, 3.2 mm, 3.4 mm,

Table 2. The electric conductivity of $SiC_f/BN/AlPO_4$/MWCNTs composites with different contents of MWCNTs.

Content of MWCNTs (wt%)	0	1.5	2.5	3.5	4.5
σ_{dc}(S/m)	8.0×10^{-6}	0.04	0.85	1.8	6.2

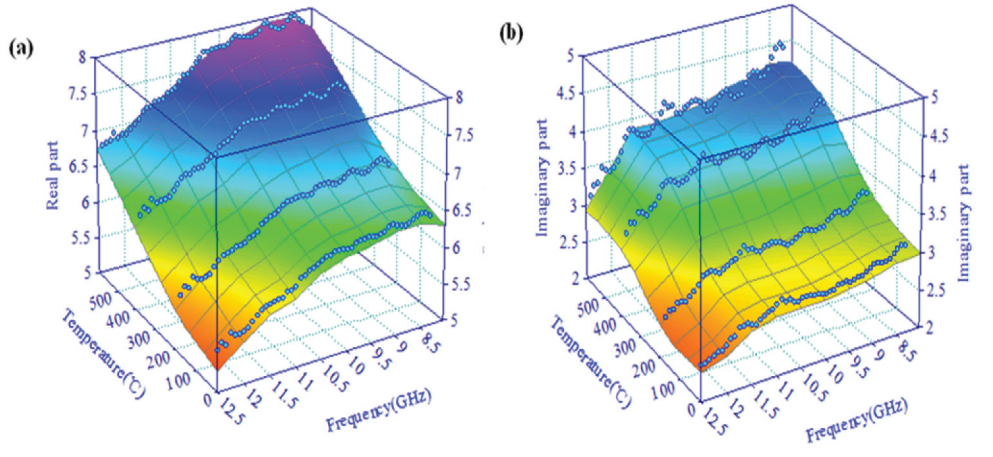

Figure 9. (a) ε′ and (b) ε″ for SiC_f/BN/$AlPO_4$/MWCNTs composites with 1.5 wt. % MWCNTs at various temperature.

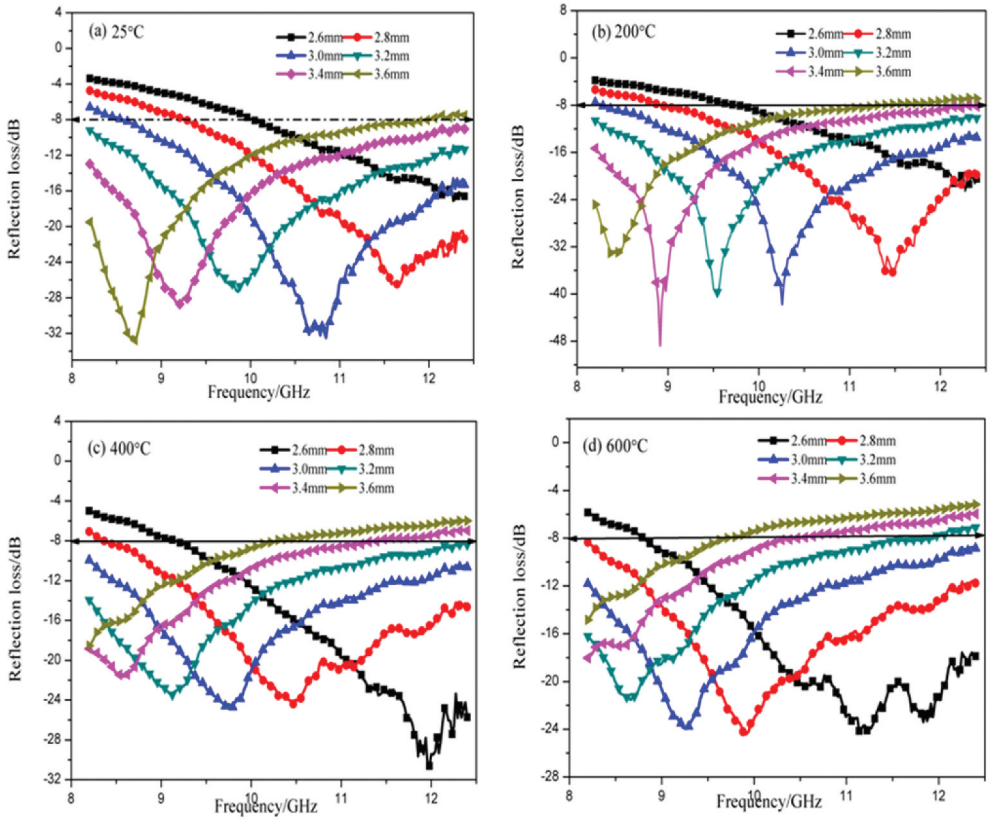

Figure 10. The reflection loss curves of various thicknesses of SiC_f/BN/$AlPO_4$/MWCNTs composites at different temperatures: (a) 25°C, (b) 200°C, (c) 400°C, and (d) 600°C.

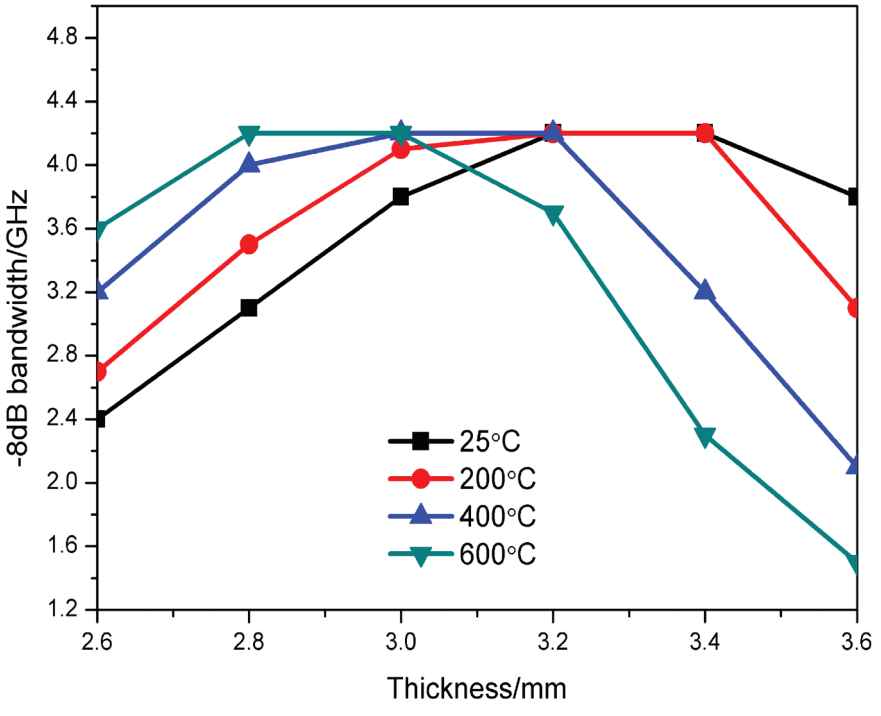

Figure 11. The-8 dB bandwidth vs. thickness curves of SiC_f/BN/$AlPO_4$/MWCNTs composites at various temperatures.

and 3.6 mm. The absorbing bandwidth below −8 dB is chosen to evaluate the microwave absorbing property of SiC_f/BN/$AlPO_4$/MWCNTs composites.

According to Figure 10, the absorbing bandwidth below −8 dB within the thickness range of 2.6–3.6 mm is shown in Figure 11 at each temperature. From Figure 10, it can be observed that when the thickness is chosen to be from 3.2 to 3.4 mm, the frequency width of reflection loss of less than −8 dB is 4.2 GHz (the entire X-band) at 25°C and 200°C. When the thickness is chosen to be from 3.0 to 3.2 mm, the frequency width of reflection loss of less than −8 dB is 4.2 GHz (the entire X-band) at 400°C. As for the 600 °C, the suitable thickness is from 2.8 to 3.0 mm. Obviously, matching thickness decreases with the increasing temperature. Even if the absorber can show excellent wave absorbing property at low temperatures, higher temperatures may worsen the property. Hence, the thickness of the SiC_f/BN/$AlPO_4$/MWCNTs composites is crucial. At a specific thickness, the composites display good absorbing wave property in the entire temperature range. It can be seen from Figure 11 when the thickness is from 3.0 to 3.2 mm, the bandwidth for −8 dB reflection loss shows minimal difference when the temperature increased from 25 to 600°C.

Microwave absorbing property are determined by two factors: impedance matching and attenuation constant. The attenuation constant has no relationship with thickness, but the impedance value is strongly dependent on the thickness. For example, when SiC_f /BN/$AlPO_4$/MWCNTs composites are prepared with 1.5 wt. % MWCNTs content and at

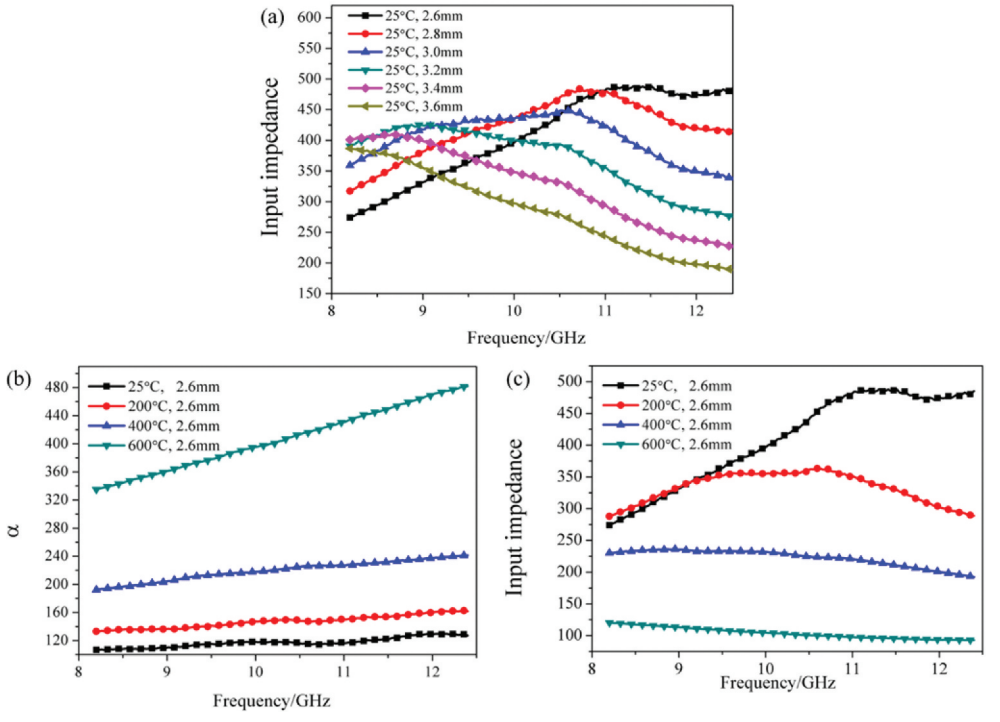

Figure 12. (a) Input impedance of SiC_f/BN/$AlPO_4$/MWCNTs composites with different thicknesses at 25°C, (b) attenuation constant and (c) input impedance of SiC_f/BN/$AlPO_4$/MWCNTs composites with 2.6 mm thickness at different temperatures.

25°C, the attenuation constant of composites is unchanged with increasing thickness. But the input impedances differ at different thicknesses, as shown in Figure 12(a). The impedance value of vacuum is 377 Ω. The closer the input impedance value of SiC_f /BN/$AlPO_4$/MWCNTs composites to the vacuum value, the more electromagnetic wave can enter the composites. When the frequency is 12.4 GHz, the input impedances at 2.8 mm, 3.0 mm, 3.2 mm, 3.4 mm, and 3.6 mm are 415 Ω, 339 Ω, 275 Ω, 226 Ω, and 188 Ω respectively. The difference between input impedances and impedance of vacuum increases gradually, less electromagnetic wave enters the material and microwave absorbing property is less poor, proved by Figure 10(a). The attenuation constant and input impedance of 2.6 mm SiC_f/BN/$AlPO_4$/MWCNTs composites prepared at different temperatures are reflected in Figure 12(b,c), respectively. Although the difference between input impedances and impedance of vacuum at 600°C is larger than that at 25°C, the attenuation constant at 600°C is far higher than that at 25°C. Thus, the microwave absorbing property at 600°C is still better than that at 25°C, as reflected in Figure 10.

Figure 13 shows the high-temperature reflection loss of SiC_f/BN/$AlPO_4$/MWCNTs composites with 3.1 mm thickness. Reflection loss of less than – 8 dB is almost in the entire X-band when the temperature changes from 25 to 600°C. Hence, the SiC_f /BN/$AlPO_4$/MWCNT composites of 3.1 mm thickness display good microwave absorbing property at high temperatures.

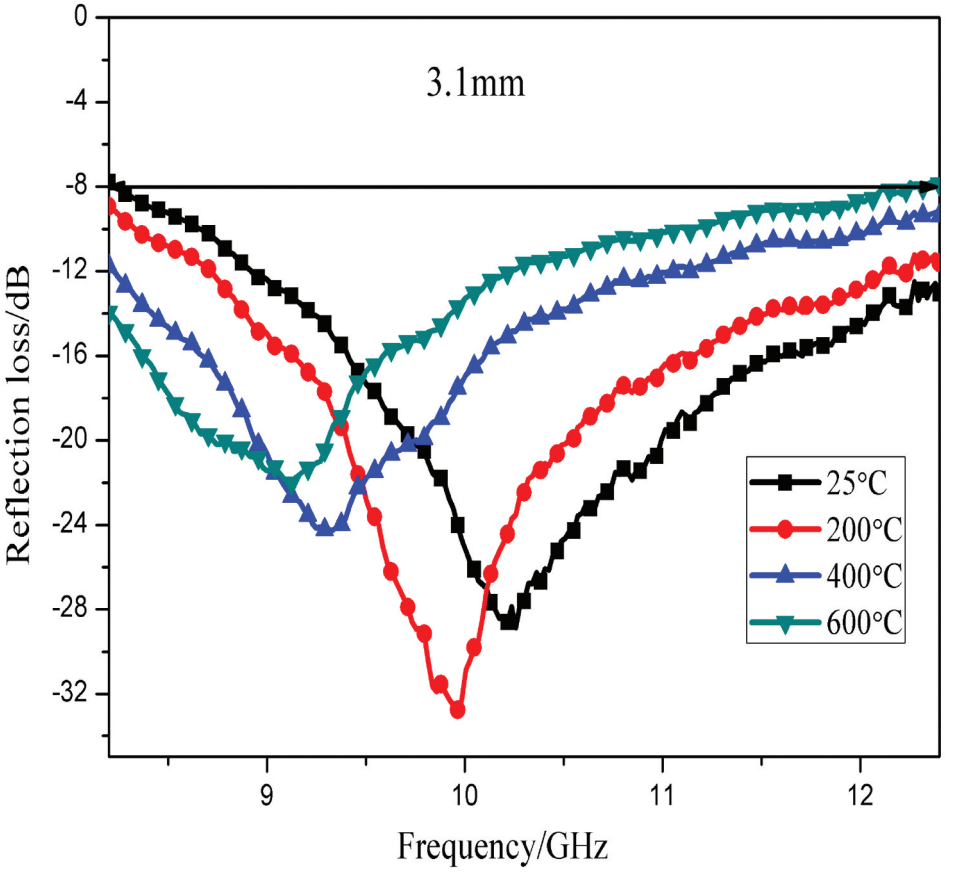

Figure 13. The reflection loss curves of 3.1-mm-thick SiC_f/BN/$AlPO_4$/MWCNTs composites at various temperatures.

4. Conclusions

(1) SiC_f/BN/$AlPO_4$/MWCNTs composites are fabricated by lamination and BN interface is successfully prepared via dip-coating method. The crystallinity of BN increases with elevated temperatures. Through the introduction of BN interface into SiC_f/BN/$AlPO_4$/MWCNT composites, there are clear improvements to the flexural strength and fracture displacement, transforming brittle fracture behavior into ductile fracture behavior.

(2) By investigating the dielectric property of SiC_f/BN/$AlPO_4$/MWCNT composites with different amounts of MWCNTs (1.5, 2.5, 3.5, and 4.5 wt. %), it is found that shortened relaxation time of electron polarization in SiC_f/BN/$AlPO_4$/MWCNT composites contribute to enhancement of ε'. As for ε″, it is controlled by relaxation time and electric conductivity. The more MWCNTs content, the greater effect electric conductivity on the ε″.

(3) The calculated reflection loss indicates that microwave-absorption property is remarkably affected by impedance match and electromagnetic attenuation. It is

tightly correlated with the electromagnetic parameters, absorber thickness, temperature, and frequency. By adjusting MWCNTs content to 1.5 wt. % and composites thickness to 3.1 mm, the reflection loss of less than −8 dB for SiC_f/BN/$AlPO_4$/MWCNTs composites is almost in the entire X-band when the temperature increases from 25 to 600°C.

Excellent mechanical property and wave absorbing property elucidate that SiC_f/BN/$AlPO_4$/MWCNT composites are possible be used as structural electromagnetic wave absorbing materials in high-temperature environment.

Disclosure statement

No potential conflict of interest was reported by the authors.

Funding

This work is jointly supported by National Natural Science Foundation of China (Grant No. 51802095), the Natural Science Foundation of Hunan Province (Grant No. 2019JJ50165).

ORCID

Feng Wan http://orcid.org/0000-0003-3038-7376

References

[1] Wang H, Zhu D, Wang X, et al. Influence of silicon carbide fiber (SiC_f) type on the electromagnetic microwave absorbing properties of SiC_f/epoxy composites. Compos Part A Appl S. 2017;93:10–17.
[2] Zhao T, Jin W, Ji X, et al. Synthesis of sandwich microstructured expanded graphite/barium ferrite connected with carbon nanotube composite and its electromagnetic wave absorbing properties. J Alloy Compd. 2017;712:59–68.
[3] Zhang Q, Gou Y, Wang J, et al. Preparation and characterization of polymer-derived Zr/Si/C multiphase ceramics and microspheres with electromagnetic wave absorbing capabilities. J Eur Ceram Soc. 2017;37:1909–1916.
[4] Shao T, Ma H, Wang J, et al. High temperature absorbing coatings with excellent performance combined Al_2O= and TiC material. J Eur Ceram Soc. 2020;40:2013–2019.
[5] Cheng Z, Liu Y, Ye F, et al. Microstructure and EMW absorbing properties of SiC_{nw}/SiBCN-Si_3N_4 ceramics annealed at different temperatures. J Eur Ceram Soc. 2020;40:1149–1158.
[6] Zhao M, Liu Y, Chai N, et al. Effect of SiBCN content on the dielectric and EMW absorbing properties of SiBCN-Si_3N_4 composite ceramics. J Eur Ceram Soc. 2018;38:1334–1340.
[7] Mo R, Yin X, Ye F, et al. Electromagnetic wave absorption and mechanical properties of silicon carbide fibers reinforced silicon nitride matrix composites. J Eur Ceram Soc. 2019;39:743–754.
[8] Tian H, Liu HT, Cheng HF. A high-temperature radar absorbing structure: design, fabrication, and characterization. Compos Sci Technol. 2014;90:202–208.
[9] Cao MS, Song WL, Hou ZL, et al. The effects of temperature and frequency on the dielectric properties, electromagnetic interference shielding and microwave-absorption of short carbon fiber/silica composites. Carbon. 2010;48:788–796.

[10] Li M, Yin X, Zheng G, et al. High-temperature dielectric and microwave absorption properties of Si_3N_4–SiC/SiO_2 composite ceramics. J Mater Sci. 2015;50:1478–1487.
[11] Kong L, Yin X, Li Q, et al. High-temperature electromagnetic wave absorption properties of ZnO/$ZrSiO_4$ composite ceramics. J Am Ceram Soc. 2013;96:2211–2217.
[12] Wen B, Cao MS, Hou ZL, et al. Temperature dependent microwave attenuation behavior for carbon-nanotube/silica composites. Carbon. 2013;65:124–139.
[13] Han M, Yin X, Duan W, et al. Hierarchical graphene/SiC nanowire networks in polymer-derived ceramics with enhanced electromagnetic wave absorbing capability. J Eur Ceram Soc. 2016;36:2695–2703.
[14] Liu H, Tian H. Mechanical and microwave dielectric properties of SiC_f/SiC composites with BN interphase prepared by dip-coating process. J Eur Ceram Soc. 2012;32:2505–2512.
[15] Yang B, Zhou X, Chai Y. Mechanical properties of SiC_f/SiC composites with PyC and the BN interface. Ceram Int. 2015;41:7185–7190.
[16] Tian H, Liu HT, Cheng HF. Mechanical and microwave dielectric properties of KD-I SiC_f /SiC composites fabricated through precursor infiltration and pyrolysis. Ceram Int. 2014;40:9009–9016.
[17] Mu Y, Zhou W, Hu Y, et al. Improvement of mechanical and dielectric properties of PIP-SiC_f/SiC composites by using Ti_3SiC_2 as inert filler. Ceram Int. 2015;41:4199–4206.
[18] Huang Z, Kang W, Qing Y, et al. Influences of SiC_f content and length on the strength, toughness and dielectric properties of SiC_f/LAS glass-ceramic composites. Ceram Int. 2013;39:3135–3140.
[19] Wan F, Luo F, Wang H, et al. Effects of carbon black (CB) and alumina oxide on the electromagnetic- and microwave-absorption properties of SiC fiber/aluminum phosphate matrix composites. Ceram Int. 2014;40:15849–15857.
[20] Hu Y, Luo F, Yang Z, et al. Improvement dielectric and microwave properties of SiC_f/SiC-$AlPO_4$ composites prepared by precursor infiltration and pyrolysis process. J Alloy Compd. 2017;699:498–504.
[21] Wan F, Luo F, Mu Y, et al. Enhanced mechanical and microwave-absorption properties of SiC_f/$AlPO_4$ composite with PIP–SiC interphase and the MWCNTs filler. Ceram Int. 2015;41:9957–9965.
[22] Liu H, Cheng H, Wang J, et al. Dielectric properties of the SiC fiber-reinforced SiC matrix composites with the CVD SiC interphases. J Alloy Compd. 2010;491:248–251.
[23] Mu Y, Zhou W, Wang H, et al. Mechanical and dielectric properties of 2.5D SiC_f/SiC–Al_2O_3 composites prepared via precursor infiltration and pyrolysis. Mat Sci Eng A Struct. 2014;596:64–70.
[24] Mu Y, Zhou W, Ding D, et al. Influence of dip-coated boron nitride interphase on mechanical and dielectric properties of SiC_f/SiC composites. Mat Sci Eng A Struct. 2013;578:72–79.
[25] Wan F, Yan J, Xu H. Enhanced microwave absorbance of oxidized SiC_f/$AlPO_4$ composites via the formation of a carbon layer on the SiC fibre surface. J Eur Ceram Soc. 2018;38:4356–4362.
[26] Chollon G, Pailler R, Canet R, et al. Correlation between microstructure and electrical properties of SiC-based fibres derived from organosilicon precursors. J Eur Ceram Soc. 1998;18:725–733.
[27] Thomas J, Weston NE, O'Connor TE. Turbostratic1 boron nitride, thermal transformation to ordered-layer-lattice boron nitride. J Am Ceram Soc. 1962;84:4619–4622.
[28] Wang X, Xie Y, Guo Q. Synthesis of high quality inorganic fullerene-like BN hollow spheres via a simple chemical route. Chem Commun. 2003;2688–2689. DOI:10.1039/b308264d
[29] Hamilton EJM, Dolan SE, Mann CM, et al. Preparation of amorphous boron nitride from the reaction of haloborazines with alkali metals and formation of a novel tubular morphology by thermal annealing. Chem Mater. 1995;7:111–117.
[30] Huang Z, Zhou W, Ma R, et al. Dielectric and mechanical properties of hot-pressed sintered C_{sf}/Al_2O_3 ceramic composites. Int J Appl Ceram Tech. 2011;9:413–420.

[31] Li C, Thostenson ET, Chou TW. Dominant role of tunneling resistance in the electrical conductivity of carbon nanotube–based composites. Appl Phys Lett. 2007;91:223114.
[32] Li C, Thostenson ET, Chou TW. Effect of nanotube waviness on the electrical conductivity of carbon nanotube-based composites. Compos Sci Technol. 2008;68:1445–1452.
[33] Namouchi F, Jilani W, Guermazi H. Thermally stimulated depolarization current and dielectric spectroscopy used to study dipolar relaxations and trap level distribution in PMMA polymer. J Non-Cryst Solids. 2015;427:76–82.